Bergische Universität Wuppertal

Fachbereich Mathematik und Naturwissenschaften

Lehrstuhl für Angewandte Mathematik
und Numerische Mathematik

Preprint BUW-AMNA 06/08

Andreas Bartel, Stephanie Knorr and Roland Pulch

Wavelet-based Adaptive Grids for Multirate Partial Differential-Algebraic Equations

December 2006

http://www.math.uni-wuppertal.de/org/Num/

Wavelet-based Adaptive Grids for Multirate Partial Differential-Algebraic Equations

A. Bartel, S. Knorr, R. Pulch

Bergische Universität Wuppertal, Fachbereich C, Lehrstuhl Angewandte Mathematik/Numerische Mathematik, Gaußstr. 20, D-42119 Wuppertal, Germany. Email: [bartel,knorr,pulch]@math.uni-wuppertal.de

Abstract

The mathematical model of electric circuits yields systems of differential-algebraic equations (DAEs). In radio frequency applications, a multivariate model of oscillatory signals transforms the DAEs into a system of multirate partial differential-algebraic equations (MPDAEs). Considering quasiperiodic signals, an approach based on a method of characteristics yields efficient numerical schemes for the MPDAEs in time domain. If additionally digital signal structures arise, an adaptive grid is required to achieve the efficiency of the technique. We present a strategy applying a wavelet transformation to construct a mesh for resolving steep gradients in respective signals. Consequently, we employ finite difference methods to determine an approximative solution of characteristic systems in according grid points. Numerical simulations demonstrate the performance of the adaptive grid generation, where radio frequency signals with digital structures are resolved.

1 Introduction

In the field of telecommunication electronics, we have to deal with oscillatory signals composed of multiple frequencies. For instance, some pieces of information are represented by a slowly varying amplitude of a high frequency carrier signal. Thus we have signals which exhibit largely differing time scales. To sample these waveforms in time domain, we need to resolve the fast carrier, which determines the step size of an integration scheme, whereas the slowly varying component fixes our simulation horizon (the time interval, for which we want to compute the waveforms of the network). The introduction of multiple time variables for the occurring scales enables a more adequate formulation, where the waveforms are

represented by multivariate functions. For quasiperiodic waveforms, which arise in radio frequency (RF) applications, this representation is much more suited for an efficient sampling.

The numerical simulation of electrical circuits is based on a network approach, which typically yields systems of differential-algebraic equations (DAEs) [5]. By introducing the multivariate signal representations, partial differential-algebraic equations are deduced [2], which we further transform and then solve more efficiently. The network model and its multivariate transformation are presented in Section 2. Then, in Section 3, we discuss a method of characteristics, which is used to solve these systems [11]. In this work, the corresponding technique will be based on a finite difference method (FDM).

In addition, we have to cope with digital-like (or pulsed) signals. For instance, steep gradients are often observed in clock signals or by the extraction of digital components using thresholds. Thus heterogeneous waveforms arise in the DAE network equation. To extract efficiently the locations of steep gradients, we apply a wavelet transformation for a simple representation (analysis) of digital-like signals in Section 4. Consequently, we develop a strategy to generate an adaptive grid for applying the method of characteristics.

For numerical tests, we use this adaptive method to a circuit, the so-called Schmitt trigger, which implements a modulation of a pulse width, and discuss the numerical results in Section 5.

2 MPDAE Model

To demonstrate the multivariate model, we consider the multitone signal

$$v(t) := \left[1 + \alpha \sin\left(\frac{2\pi}{T_1} t\right)\right] \sin^2\left(\frac{\pi}{T_2} t\right) \tag{1}$$

with time scales $T_1 > T_2$. The parameter $\alpha \in (0, 1)$ controls the size of an amplitude modulation for a high-frequency oscillation. Fig. 1 (left) illustrates the arising signal in case of $\alpha = 0.2$, $T_1 = 1$, $T_2 = 0.05$. In RF applications, it holds $T_1 \gg T_2$ and thus a huge number of oscillations occurs in the time interval $[0, T_1]$. Hence we require many time points to resolve the signal sufficiently accurate by a mesh in time domain.

On the contrary, we introduce an own variable for each separate time scale, which yields the multivariate function (MVF)

$$\hat{v}(t_1, t_2) := \left[1 + \alpha \sin\left(\frac{2\pi}{T_1} t_1\right)\right] \sin^2\left(\frac{\pi}{T_2} t_2\right) \tag{2}$$

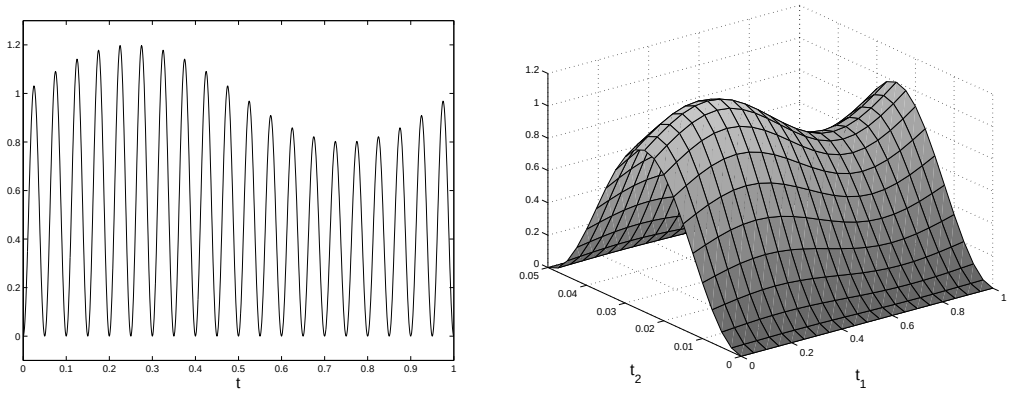

Figure 1: Amplitude modulated signal (left) and corresponding MVF (right).

of the multitone signal (1). The MVF is biperiodic and thus just determined by its values in the rectangle $[0, T_1[\times[0, T_2[$, see Fig. 1 (right). Since the MVF (2) exhibits an elementary behavior in this rectangle, we can resolve this representation sufficiently accurate using a relatively low number of mesh points. Nevertheless, we reconstruct the original signal (1) completely via

$$v(t) = \hat{v}(t, t), \tag{3}$$

i.e., the signal is located inside the MVF (2) along the diagonal $t_1 = t_2$. Therefore we achieve an efficient model of the multitone signal, since the separate time scales are decoupled in the multivariate representation. In other words, the representation (2) is independent of the ratio T_1/T_2.

More general, the multivariate model can be applied for m-tone quasiperiodic functions $x : \mathbb{R} \to \mathbb{R}$ of the form

$$x(t) = \sum_{j_1,\ldots,j_m=-\infty}^{+\infty} X_{j_1,\ldots,j_m} \exp\left(\mathrm{i}2\pi\left(\frac{j_1}{T_1} + \cdots + \frac{j_m}{T_m}\right)t\right) \tag{4}$$

with coefficients $X_{j_1,\ldots,j_m} \in \mathbb{C}$. The corresponding MVF $\hat{x} : \mathbb{R}^m \to \mathbb{R}$ reads

$$\hat{x}(t_1, \ldots, t_m) = \sum_{j_1,\ldots,j_m=-\infty}^{+\infty} X_{j_1,\ldots,j_m} \exp\left(\mathrm{i}2\pi\left(\frac{j_1 t_1}{T_1} + \cdots + \frac{j_m t_m}{T_m}\right)\right), \tag{5}$$

which is periodic in each time scale. Furthermore, efficient representations exist for envelope modulated signals using MVFs, too, where the slowest time scale is aperiodic, see [14]. The reconstruction of the signal (4) applies

$$x(t) = \hat{x}(t, \ldots, t)$$

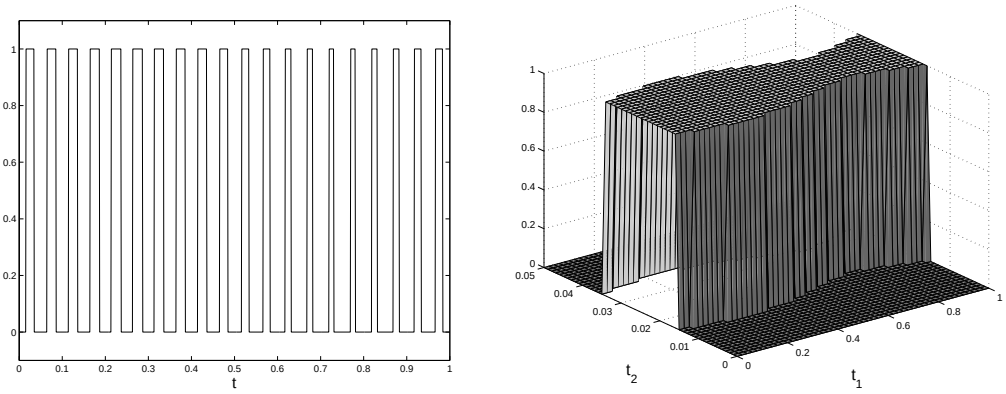

Figure 2: Digital signal (left) and corresponding MVF (right).

and the efficiency follows from the periodicities of the MVF (5).

We focus on the computation of quasiperiodic signals (4) with digital structures. Thereby, we restrict to the most frequent case of two-tone signals ($m = 2$), since generalizations to several time scales are straightforward. For an according example, let $s : \mathbb{R} \to \mathbb{R}$ be a smooth time-dependent signal. Consequently,

$$w(t) := \begin{cases} 1, & \text{for } s(t) > \eta \\ 0, & \text{for } s(t) \leq \eta \end{cases} \tag{6}$$

is a corresponding digital version, where we apply some threshold value $\eta \in \mathbb{R}$. Considering signal (1) for s and $\eta := 0.7$, we obtain the function (6) shown in Fig. 2 (left). Here, the amplitude modulation in (1) causes a modulation of the pulse width in (6). The corresponding MVF is presented in Fig. 2 (right). We recognize that discontinuities arise in the multitone signal as well as in the MVF. If such an MVF is computed numerically using a grid in the domain of dependence, the mesh has to be refined to obtain a sufficiently accurate approximation. Thereby, the refinement is necessary only near the discontinuities, whereas a coarse grid is adequate elsewhere. The same problem occurs for smooth signals with extremely steep gradients localized at certain time points. However, the efficiency of the multivariate model can still be achieved via appropriate generation of meshes.

Now we consider the corresponding model of electric circuits. Typically, the mathematical description of circuits results from a network approach, where several variants exist differing mainly in the set of involved unknowns. Thereby, the transient behavior of (nearly all) node voltages, branch currents and possibly other quantities like charges and fluxes are analyzed. In general, systems of differential-algebraic equations arise in each variant of the network approach. For

example, a common charge-oriented version, see [5], yields the following system

$$\begin{aligned} A_C \tfrac{\mathrm{d}}{\mathrm{d}t}\tilde{\mathbf{q}} + A_R \mathbf{r}(A_R^\top \mathbf{u}(t), t) + A_L \boldsymbol{\jmath}_L(t) + A_V \boldsymbol{\jmath}_V(t) + A_I \boldsymbol{\imath}(t) &= \mathbf{0}, \\ \tfrac{\mathrm{d}}{\mathrm{d}t}\tilde{\boldsymbol{\Phi}} - A_L^\top \mathbf{u}(t) &= \mathbf{0}, \\ A_V^\top \mathbf{u}(t) - \mathbf{v}(t) &= \mathbf{0}, \\ \tilde{\mathbf{q}} - \mathbf{q}_C(A_C^\top \mathbf{u}(t), t) &= \mathbf{0}, \\ \tilde{\boldsymbol{\Phi}} - \boldsymbol{\Phi}_L(\boldsymbol{\jmath}_L(t), t) &= \mathbf{0}. \end{aligned} \tag{7}$$

The incidence matrices A_C, A_R, A_L and A_V, A_I belong to capacitive, resistive, inductive parts of the network and to branches with independent voltage and current sources, respectively. Furthermore, we obtain the function $\mathbf{r}$ for resistances, $\boldsymbol{\imath}$ for current sources and $\mathbf{v}$ for voltage sources. The state variables $\tilde{\mathbf{q}}, \tilde{\boldsymbol{\Phi}}, \mathbf{u}, \boldsymbol{\jmath}_L, \boldsymbol{\jmath}_V$ represent charges, fluxes, node potentials and currents through inductances and voltage sources.

Using the notation

$$\mathbf{x} := (\tilde{\mathbf{q}}, \tilde{\boldsymbol{\Phi}}, \mathbf{u}, \boldsymbol{\jmath}_L, \boldsymbol{\jmath}_V)^\top, \quad \mathbf{q}(\mathbf{x}) := (A_C\tilde{\mathbf{q}}, \tilde{\boldsymbol{\Phi}}, \mathbf{0}, \mathbf{0}, \mathbf{0})^\top,$$

we write system (7) in the compact form

$$\frac{\mathrm{d}\mathbf{q}(\mathbf{x})}{\mathrm{d}t} = \mathbf{f}(\mathbf{b}(t), \mathbf{x}(t)) \tag{8}$$

with unknown function $\mathbf{x} : \mathbb{R} \to \mathbb{R}^k$, the function $\mathbf{q} : \mathbb{R}^k \to \mathbb{R}^k$ and general right-hand side $\mathbf{f} : \mathbb{R}^l \times \mathbb{R}^k \to \mathbb{R}^k$. The function $\mathbf{b} : \mathbb{R} \to \mathbb{R}^l$ includes independent input signals. Initial value problems of (8) require a consistent starting value $\mathbf{x}(t_0) = \mathbf{x}_0$ and are solved over some time interval $t \in [t_0, t_1]$. However, the task is often to determine the steady state response of an electric circuit, which corresponds to periodic or quasiperiodic solutions, for example. Hence two-point or multi-point boundary value problems of (8) arise, respectively.

Alternative mathematical models of electric circuits often result in systems of type (8), too. An advantage of the approach (7) consists in the conservation of charges. Furthermore, the left-hand side of (8) does not depend explicitly on time in that case. However, the Jacobian matrix of $\mathbf{q}$ is usually singular in each network approach, which leads to differential-algebraic equations.

We assume that the input $\mathbf{b}$ consists of two-tone quasiperiodic signals (4). The output $\mathbf{x}$ often inherits this time behavior and thus is considered as quasiperiodic, too. In RF applications, the corresponding time rates T_1, T_2 are widely separated. A numerical integration scheme for solving the DAEs (8) involves a huge computational effort, since the fast oscillations restrict the step sizes in time, whereas the slow part determines the total time interval of the simulation. The computation of a circuit's steady state response, i.e., a quasiperiodic solution of (8),

implies analog difficulties. Consequently, we apply biperiodic MVFs $\hat{\mathbf{b}}$ and $\hat{\mathbf{x}}$ of type (5) with $m = 2$ for the signals $\mathbf{b}$ and $\mathbf{x}$. Brachtendorf et al. [2] transformed the system of DAEs (8) into a system of multirate partial differential-algebraic equations (MPDAEs)

$$\frac{\partial \mathbf{q}(\hat{\mathbf{x}})}{\partial t_1} + \frac{\partial \mathbf{q}(\hat{\mathbf{x}})}{\partial t_2} = \mathbf{f}(\hat{\mathbf{b}}(t_1, t_2), \hat{\mathbf{x}}(t_1, t_2)). \tag{9}$$

If $\hat{\mathbf{x}}$ is an arbitrary solution of this system, then the restriction $\mathbf{x}(t) := \hat{\mathbf{x}}(t, t)$ following (3) satisfies the DAE (8). For electric networks using model (7), the MPDAE inherits properties of the original DAE like the index concepts, see [9].

The quasiperiodicity implies periodicity conditions of the MVFs in multidimensional time domain

$$\hat{\mathbf{x}}(t_1, t_2) = \hat{\mathbf{x}}(t_1 + T_1, t_2) = \hat{\mathbf{x}}(t_1, t_2 + T_2), \quad \text{for all } \; t_1, t_2 \in \mathbb{R}, \tag{10}$$

where the time scales T_1, T_2 are known from the input signals. Consequently, we solve the MPDAE system numerically in a bounded domain like the rectangle $[0, T_1] \times [0, T_2]$, for example, instead of performing a transient integration of the corresponding DAE system. For envelope modulated signals, initial-boundary value problems of the system (9) arise in the domain $\mathbb{R}^+ \times [0, T_2]$, cf. [14].

The MPDAE model (9) for DAEs (8) can be used for other problems, too, where quasiperiodic or envelope-modulated signals arise. However, simulation of RF circuits represents the most common application area.

3 Method of Characteristics

To solve the MPDAE (9) with periodicity conditions (10), frequency domain methods have been successfully used in [2]. However, time domain methods exhibit a better performance for strongly nonlinear problems or digital signal structures, see [14]. The system (9) is of hyperbolic structure with characteristic curves, see [11]. The corresponding characteristic system reads

$$\frac{\mathrm{d}}{\mathrm{d}\tau} t_1(\tau) = 1, \quad \frac{\mathrm{d}}{\mathrm{d}\tau} t_2(\tau) = 1, \quad \frac{\mathrm{d}}{\mathrm{d}\tau} \mathbf{q}(\bar{\mathbf{x}}(\tau)) = \mathbf{f}(\hat{\mathbf{b}}(t_1(\tau), t_2(\tau)), \bar{\mathbf{x}}(\tau)), \tag{11}$$

where the variables t_1, t_2 as well as the solution $\bar{\mathbf{x}}$ depend on a parameter τ. Solutions of this system are called characteristic curves. The equations for the variables t_1, t_2 can be solved explicitly and yield parallel characteristic projections in diagonal direction. Inserting the result in the last part of (11), we obtain

$$\frac{\mathrm{d}}{\mathrm{d}\tau} \mathbf{q}(\bar{\mathbf{x}}(\tau)) = \mathbf{f}(\hat{\mathbf{b}}(\tau + c_1, \tau + c_2), \bar{\mathbf{x}}(\tau)) \tag{12}$$

with arbitrary constants $c_1, c_2 \in \mathbb{R}$ and $\bar{\mathbf{x}}(\tau) = \hat{\mathbf{x}}(\tau + c_1, \tau + c_2)$. This system represents a family of DAEs, which describes the transport of information in the MPDAE system completely.

In view of the periodicity conditions (10), we consider the corresponding rectangle $[0, T_1] \times [0, T_2]$ in the domain of dependence. Without loss of generality, we assume $T_1 > T_2$. Choosing equidistant initial points on the line $t_2 = 0$ results in the discretization

$$\bar{\mathbf{x}}_{j_1}(\tau) := \hat{\mathbf{x}}(\tau + (j_1 - 1)h_1, \tau), \quad \text{for } \; j_1 = 1, \ldots, n_1 \tag{13}$$

using some step size $h_1 = T_1/n_1$. Fig. 3 illustrates the involved characteristic projections with the respective transport of information indicated by arrows as well as the diagonal $t_1 \equiv t_2 \mod T_2$ (dotted line). In the figure, the case of $T_1 \gg T_2$ is sketched qualitatively (not quantitatively). The projections according to (13) do not necessarily coincide with the diagonal line. However, this fact does not result in significant disadvantages. The equations corresponding to (13) from the family (12) are

$$\frac{\mathrm{d}}{\mathrm{d}\tau}\mathbf{q}(\bar{\mathbf{x}}_{j_1}(\tau)) = \mathbf{f}(\hat{\mathbf{b}}(\tau + (j_1 - 1)h_1, \tau), \bar{\mathbf{x}}_{j_1}(\tau)), \quad \text{for } \; j_1 = 1, \ldots, n_1 \tag{14}$$

and we consider $\tau \in [0, T_2]$. The periodicity in the fast time scale, see (10), does not yield a periodic boundary condition for the solution of (14), since the progress in diagonal direction causes a displacement. Nevertheless, applying an interpolation scheme on the line $t_2 = T_2$ generates approximative boundary conditions for the functions (13), see [11], which read

$$(\bar{\mathbf{x}}_0(0)^\top, \ldots, \bar{\mathbf{x}}_{n_1}(0)^\top)^\top = B(\bar{\mathbf{x}}_0(T_2)^\top, \ldots, \bar{\mathbf{x}}_{n_1}(T_2)^\top)^\top. \tag{15}$$

The entries of the constant matrix $B \in \mathbb{R}^{n_1 k \times n_1 k}$ depend only on the ratio T_1/T_2, the step size h_1 and the used interpolation formula. In case of $T_1 \gg T_2$, which usually implies $h_1 > T_2$, linear interpolation reads

$$\bar{\mathbf{x}}_{j_1}(0) = \left(1 - n_1\frac{T_2}{T_1}\right)\bar{\mathbf{x}}_{j_1}(T_2) + \left(n_1\frac{T_2}{T_1}\right)\bar{\mathbf{x}}_{j_1-1}(T_2), \quad \text{for } \; j_1 = 1, \ldots, n_1, \tag{16}$$

where the periodicity in the slow rate is applied to identify $\bar{\mathbf{x}}_0 = \bar{\mathbf{x}}_{n_1}$. With $T_1 \gg T_2$, the idealization $T_2/T_1 \doteq 0$ seems advantageous, since (16) would change into periodic boundary conditions. However, using this strategy, an insufficient accuracy has been observed at the boundaries, which indicates that the small displacement T_2/T_1 can not be neglected.

If digital signal structures arise, we assume that corresponding steep gradients are not situated on the boundary line $t_2 = T_2$, where the interpolation takes place (see Fig. 3). Thus a relatively small number n_1 of characteristic curves is

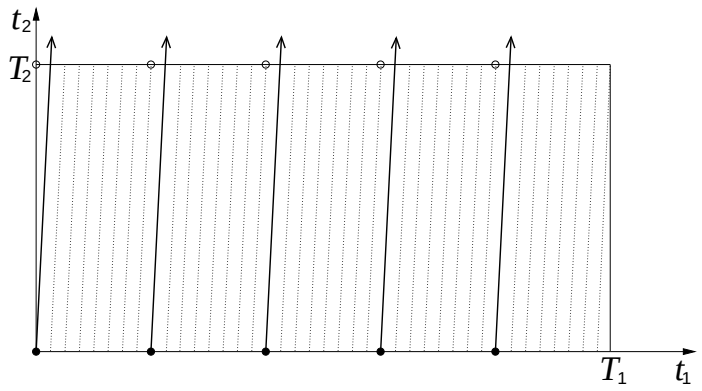

Figure 3: Characteristic projections in domain of dependence for rates $T_1 \gg T_2$.

sufficient. This requirement is satisfied by the example presented in the previous section. If the quasiperiodic solution of (8) exhibits steep gradients at $t_2 = T_2$, then considering a shifted domain $[0, T_1] \times [c, c + T_2]$ for some $c \in (0, T_2)$ with the analog boundary value problem often avoids this difficulty.

Hence the method of characteristics leads to a boundary value problem of DAEs (14-15), which can be solved by finite difference methods or shooting methods, for example. The functions (13) yield an approximation of the MPDAE solution in the corresponding rectangle, depicted in Fig. 3, and thus everywhere in view of the periodicities.

In the boundary value problem, the DAE subsystems in (14) of dimension k are separate and coupled only by the boundary condition (15). On the contrary, a finite difference method applied directly to the MPDAE (9) performs an unnecessary coupling in both coordinate directions. Therefore methods based on the problem (14-15) achieve more efficiency in comparison to standard time domain methods for the system (9), see [11, 12].

In [12], finite difference methods reproduce successfully the solution of boundary value problems (14-15). Thereby, an equidistant mesh is considered, which is sufficient for computing elementary MVFs. In contrast, digital structures cause inaccurate results on coarse grids due to steep gradients. However, the multidimensional strategy is only adequate, if a relatively low number of mesh points is sufficient. Thus we need an adaptive grid for the approach (14-15) in case of numerical methods employing the time domain.

4 Wavelet-based Adaptive Grid Generation

We aim at the detection of steep gradients in the solution for the generation of an adaptive grid. Due to the pulsed waveforms in the circuits we are considering, it is fruitful to employ ansatz functions of low order. Furthermore, the use of wavelets allows us both time and frequency localization (whereas Fourier transforms are designed for frequency extraction, only): With the so-called 'mother-wavelet' ψ, the wavelet-transform T of a signal s reads

$$\big(Ts\big)(a,b) = |a|^{-1/2} \int_{\mathbb{R}} s(t)\, \psi\left(\tfrac{t-b}{a}\right) \mathrm{d}t,$$

with dilation parameter $a \neq 0$ for the frequency range and translation parameter b for time centering (localization). For our purpose, the common hat-functions[1] are an adequate choice, which we use as wavelets from now on.

Next, we employ these ansatz functions for the discretization of the characteristic system (14) along one characteristic projection (with $\tau \in [0, T_2]$). To construct a multiresolution analysis of $L^2([0,T_2])$, we restrict the basis functions to a bounded domain $[0, L]$ by 'folding' the hat-functions at the interval boundaries, see [4]. The parameter $L \in \mathbb{N}$ defines the number of dilated basis functions on the bounded domain, which is then of course transformed to the desired interval $[0, T_2]$. Without loss of generality, we demand $\operatorname{supp}\psi \subseteq [0, L]$.

For our numerical approximation, we use a subspace $V_J^{[0,L]} \subset L^2([0,L])$ of finite dimension, which is composed by a direct sum of a central space $V_0^{[0,L]}$ (spanned by integer translates of the scaling function[2]) and hat-wavelet spaces $W_j^{[0,L]}$ with according frequency localizations:

$$V_J^{[0,L]} = V_0^{[0,L]} \oplus \bigoplus_{j=0}^{J-1} W_j^{[0,L]}.$$

Due to the bounded domain, the number of translations $k \in \mathcal{I}_j \subset \mathbb{N}$ spanning the spaces $W_j^{[0,L]}$ is finite:

$$W_j^{[0,L]} = \operatorname{span}\big\{\psi_{j,k} \,|\, \psi_{j,k}(\tau) := 2^{j/2}\psi(2^j\tau - k),\, k \in \mathcal{I}_j\big\},$$

for $j = 0, \ldots, J-1$.

Notice, in contrast to frequently used orthonormal bases, this wavelet basis is a biorthogonal system. The main difference is that for the synthesis of a wavelet-transformed signal the dual basis applies. So in our case, the dual wavelet basis

[1] The hat-functions are obtained from a so-called scaling function, which is in our case the linear B-spline.

[2] The B-spline scaling functions give us the coarsest approximation.

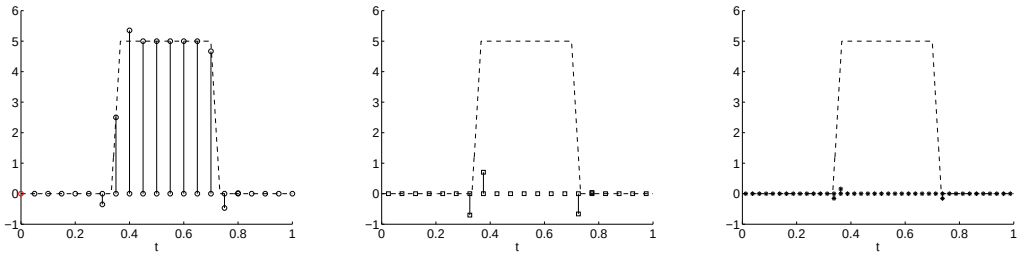

Figure 4: Pulse representation in $V_0^{[0,20]}$ (left), $W_0^{[0,20]}$ (middle) and $W_1^{[0,20]}$ (right).

in fact undertakes the time-frequency localization of the wavelet coefficients and we thus do not have to set it up explicitly. For more details on biorthogonal wavelet bases, see [3], for example.

To illustrate the capabilities of the hat-wavelets for our digital-like signals, we approximate a pulse function $p : [0, 1] \to \mathbb{R}$ in the subspace $V_2^{[0,20]}$, i.e. using the refinement of $L+1 = 21$ basis functions in the central space. The pulse function p is given in Fig. 4 as dashed line. There we show in three plots the coefficients for the corresponding spaces $V_0^{[0,20]}$, $W_0^{[0,20]}$ and $W_1^{[0,20]}$, respectively. The different markers indicate the size of these coefficients versus the corresponding location of the hat-functions' maximal value. Thereby we obtain a dyadic grid for the interval $[0, L]$: the integer values

$$\tau_k = k, \quad k = 0, \ldots, L,$$

for $V_0^{[0,L]}$ and the refinements

$$\tau_k = 2^{-j}(k + 1/2), \quad k = 0, \ldots, 2^j L,$$

for $W_j^{[0,L]}$, $j = 0, 1$.

Notice that the shape of the pulse is well represented by $V_0^{[0,20]}$ (scaling functions are normalized to 1), only at the location of the steep gradients the refinement levels $W_0^{[0,20]}$, $W_1^{[0,20]}$ have contributions, but attenuate fast. Thus we can employ this localization of the steep gradients to define an adaptive grid [1]: given a guess of the solution, we perform a discrete wavelet-transformation (DWT) and 'simply' inspect the size of the corresponding coefficients. Thus grid points associated with 'small' coefficients (smaller than a given threshold) are left out and grid points are added, where the coefficients exceed a given upper threshold. Of course, the relative level of these coefficients (compared within the same subspace) is most instructive.

A guess for the solution can be obtained by an ordinary DAE simulation of (8) in normal time with initial value $\mathbf{x}_0$ for the relatively short interval $[0, T_2]$ (we

are interested in the case $T_1 \gg T_2$). Then we compute for each component of the solution the DWT, determine a grid, and use the common refinement (which means adding the discretization points of all components to a single grid). In this way, we obtain the location of the steep gradients at the starting time. If these positions do not change (over $[0, T_1]$):

$$\left\| \frac{\partial \hat{\mathbf{x}}}{\partial t_2}(0, t_2) \right\| \approx \left\| \frac{\partial \hat{\mathbf{x}}}{\partial t_2}(t_1, t_2) \right\|, \quad \text{for all } t_1 \in [0, T_1] \text{ and } t_2 \in [0, T_2],$$

we may use the same grid on all characteristic projections. An example for such a circuit is the switched capacitor filter, see [1, 8]. Similar to Fig. 3, Fig. 5 (left) gives a representation of the diagonal (dotted lines) and the selection of characteristic curves, where we are to determine the solution with identical grid on each characteristic projection.

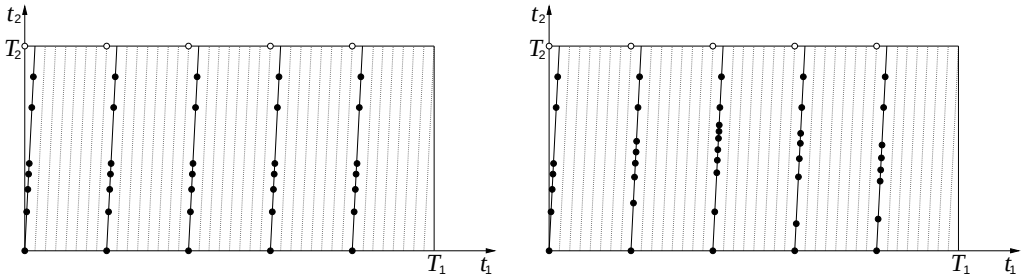

Figure 5: Adaptive characteristic grid: simple (left) and advanced (right).

Clearly, it is not sufficient to use the same grid on every characteristic projection for a signal with pulse width modulation (like in Fig. 2) or for other signals with instationary positions of the steep gradients in the t_2-direction. More severely, this will produce results of low accuracy if just the grid for the starting time is used.

To enable different grids on the characteristic curves (as in Fig. 5 (right)) and to avoid a total re-computation of the whole boundary value problem on a locally refined grid, we need also in advance information on the solutions' behavior along the characteristic projections. The crucial point is, how to determine a guess for the solution on future characteristic projections, such that we can apply the DWT. For the class of circuits, where the external signal gives rise to the positions of the steep gradients, we just solve the DAEs (14) for this future intervals by an ordinary DAE integration scheme. As initial value for a first guess, any consistent choice is sufficient. To this end, we simply perform a single step of the implicit Euler and achieve an approximative consistent solution, which is used as initial value for the respective DAE.

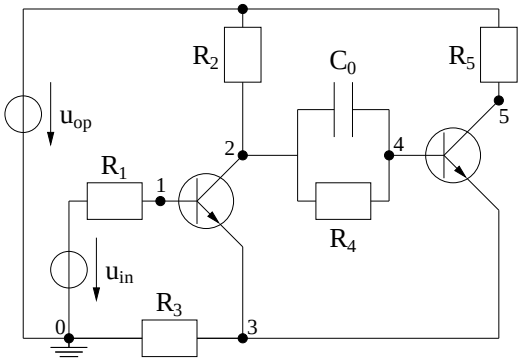

Figure 6: Schmitt trigger circuit.

The efficiency of this procedure lies in the fact that we only need the time-integration along a small number of characteristic projections, whereas a huge number of characteristics would have to be solved in ordinary time (cf. the diagonal in Fig. 5). Moreover, we solve initial value problems instead of boundary value problems and it is not necessary to solve for the limit cycle, since basically only the structure of the solution determines the adaptive grid.

Finally, with the adaptive grid at hand, we solve the boundary value problem (14-15) using a finite difference discretization described in [12].

5 Numerical Simulation

The presented method was applied to the test example of a so-called Schmitt trigger, which is depicted in Fig. 6. In this circuit, a sinusoidal input signal is transformed into a digital output signal at node 5. If the input signal exceeds the upper trigger threshold, the output signal takes the value of its upper stable state and does not jump back to its lower limit until the input falls below a lower trigger threshold. The fact that the output depends on two different thresholds and on the history of the input is called hysteresis.

The model of the used Schmitt trigger can be found in [7]. For the two npn-bipolar transistors, the current-voltage relation is given by the nonlinear function

$$g(\Delta u) := \beta \left(\exp\left(\frac{\Delta u}{u_T}\right) - 1 \right)$$

depending on the voltage drop Δu between basis and emitter with parameters $\beta = 10^{-6}\,\mathrm{A}$ and $u_T = 0.026\,\mathrm{V}$. The circuit model can be described by a differential-

algebraic system of index 1[3]:

$$C\,\tfrac{\mathrm{d}}{\mathrm{d}t}\mathbf{u} = \mathbf{f}(\mathbf{u}) + \mathbf{s}(t).$$

As special case of (8), we obtain a system with linear left-hand side and additive input signals $\mathbf{s}$. The constant capacitance matrix $C = (c_{i,j}) \in \mathbb{R}^{5\times 5}$ has the nonzero elements $c_{2,2} = c_{4,4} = C_0$ and $c_{2,4} = c_{4,2} = -C_0$. The right-hand side is given by

$$\mathbf{f}(\mathbf{u}) = \begin{pmatrix} -u_1/R_1 - (1-\alpha)g(u_1 - u_3) \\ -u_2/R_2 - (u_2 - u_4)/R_4 - \alpha g(u_1 - u_3) \\ -g(u_1 - u_3) + u_3/R_3 - g(u_4 - u_3) \\ -(u_4 - u_2)/R_4 - (1-\alpha)g(u_4 - u_3) \\ -u_5/R_5 - \alpha g(u_4 - u_3) \end{pmatrix}$$

and

$$\mathbf{s}(t) = \big(u_{in}(t)/R_1,\, u_{op}(t)/R_2,\, 0,\, 0,\, u_{op}(t)/R_5\big)^\top.$$

As the right-hand side is smooth here, we expect also the solution to be smooth with, however, very steep gradients. We use the parameters $R_1 = 200\ \Omega$, $R_2 = 1600\ \Omega$, $R_3 = 100\ \Omega$, $R_4 = 3200\ \Omega$, $R_5 = 1600\ \Omega$ and $C_0 = 40$ pF for the resistances and the capacitance, respectively, $\alpha = 0.99$ for the transistor model and the operating voltage $u_{op}(t) \equiv 0.2\,\mathrm{V}$.

We apply the two-tone quasiperiodic input signal

$$u_{in}(t) = -5\,\mathrm{V} + 10\,\mathrm{V} \cdot \left(0.8 + 0.2 \cdot \sin\left(\frac{2\pi}{T_1}t\right)\right) \cdot \sin^2\left(\frac{2\pi}{T_2}t\right)$$

with qualitatively the same structure as signal (1) in Fig. 1. To obtain an RF application, we employ $T_1 = 1\,\mathrm{s}$ and $T_2 = 5 \cdot 10^{-4}\,\mathrm{s}$. Then it holds $T_1 \gg T_2$ in contrast to the moderately separated time scales in Fig. 1. The signal $u_{in}(t)$ and its multivariate function $\hat{u}_{in}(t_1, t_2)$ are depicted in Fig. 7. Notice that the structure of the MVF here is the same as for (2); it is independent from the ratio of the time scales.

By introducing MVFs for node potentials and input signals, the network equations are transferred to the MPDAE

$$C\left(\frac{\partial \hat{\mathbf{u}}}{\partial t_1} + \frac{\partial \hat{\mathbf{u}}}{\partial t_2}\right) = \mathbf{f}(\hat{\mathbf{u}}) + \hat{\mathbf{s}}(t_1, t_2),$$

which is a special form of (9).

We solve the boundary value problem (14-15) on $n_1 = 20$ characteristic curves and apply the adaptive grid generation from the previous section with different

[3]Here no charge-oriented approach is applied and for the sake of simplicity, one node voltage has already been replaced by the value u_{op}. Thereby a more advantageous structure is achieved.

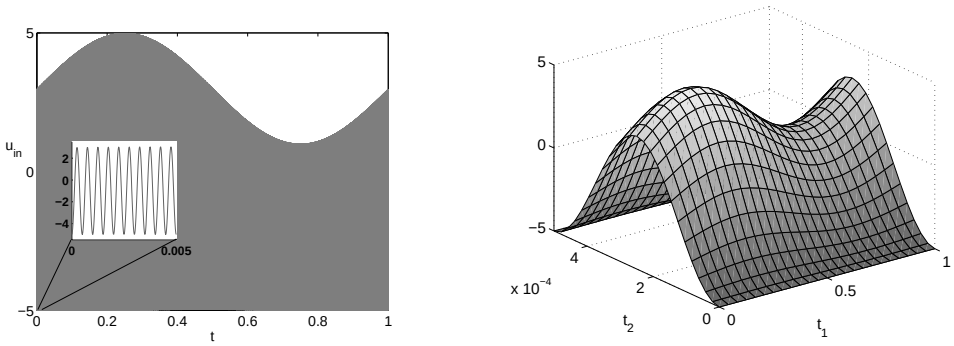

Figure 7: Input signal (left) and corresponding MVF (right).

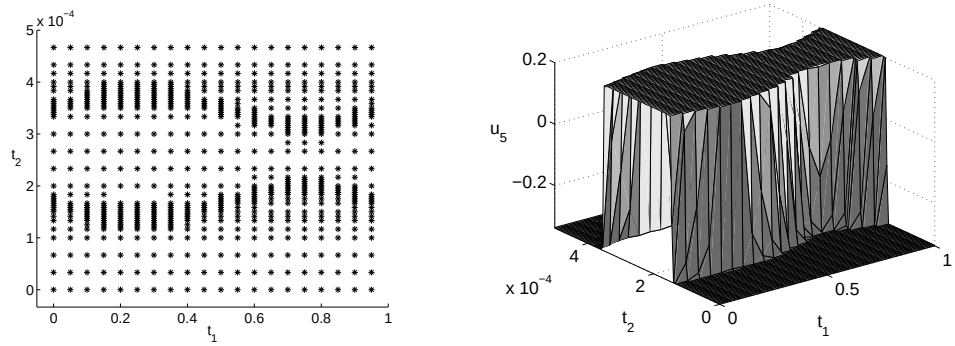

Figure 8: Adaptive grid (left) and multivariate output signal (right).

grids for each characteristic projection. Thereby we obtain a total of 711 grid points, i.e., we have on average less than $n_2 = 36$ grid points for each interval $[0, T_2]$. For the same resolution on an equidistant grid, $n_2 = 120$ points would have been necessary. The adaptive grid and the multivariate solution for the output at node 5 can be found in Fig. 8. The grid is relatively coarse except for the locations of steep gradients, which have been detected sharply by the wavelet basis. Within the finite difference discretization applied on the adaptive grid, we use the formula following Dahlquist [6]. To solve the nonlinear system arising after discretization a damped Newton method is necessary to obtain convergence.

In Fig. 9, the reconstructed DAE solution u_5 is plotted on two different sections of the whole interval $[0, T_1]$ for comparison with a standard univariate time integration based on numerical differentiation formulas (NDFs). It can be seen that the reconstucted solution (circles) coincides very well with the reference solution (solid line). We again observe a modulation of the pulse widths as explained for the signal (6).

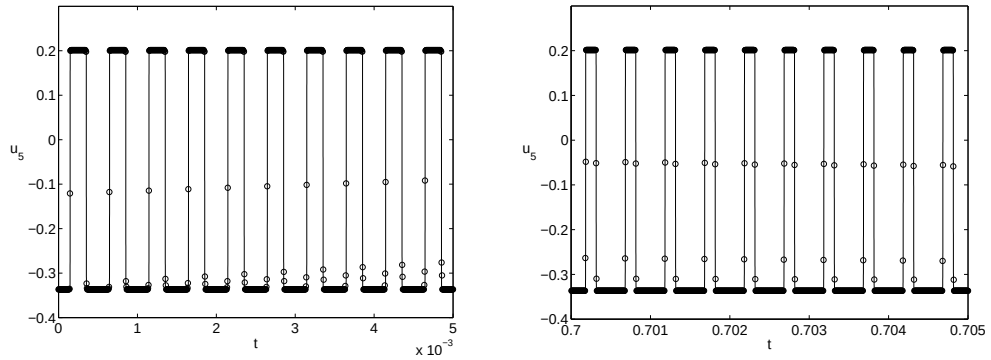

Figure 9: Reconstructed solution (circles) and reference signal (solid line) for u_5.

For the sake of completeness, the MPDAE solutions for the voltages at the nodes 1 to 4 can be found in Fig. 10. All components except the first one show steep gradients, which have been resolved by the adaptive grid.

6 Conclusions

A multidimensional modeling yields an efficient representation of RF-signals and the hyperbolic structure of the arising MPDAE network equations can be exploited to set up a method of characteristics. Moreover, the time-frequency localization property of wavelet ansatz functions is used to generate adaptive grids for the efficient solution of the arising boundary value problems along the characteristic projections. The biorthogonal basis of hat-wavelets emerged to sharply detect steep gradients of pulsed functions. This capability was verified by a successful simulation of a Schmitt trigger circuit on an adaptive grid.

In this paper, amplitude modulated signals have been investigated. The additional occurrence of frequency modulation can be addressed by a so-called warped MPDAE model as described in [10]. Having the according characteristic system to be solved, see [13], the adaptive grid generation seems to be feasible in an analog way. Anyway, the efficiency has to be investigated in detail.

A further application of the wavelet basis beyond the adaptive grid generation for the MPDAE model is to keep the wavelets as ansatz functions and solve the boundary value problems via a collocation scheme on adaptive characteristic grids. Methods of this kind are also currently being investigated.

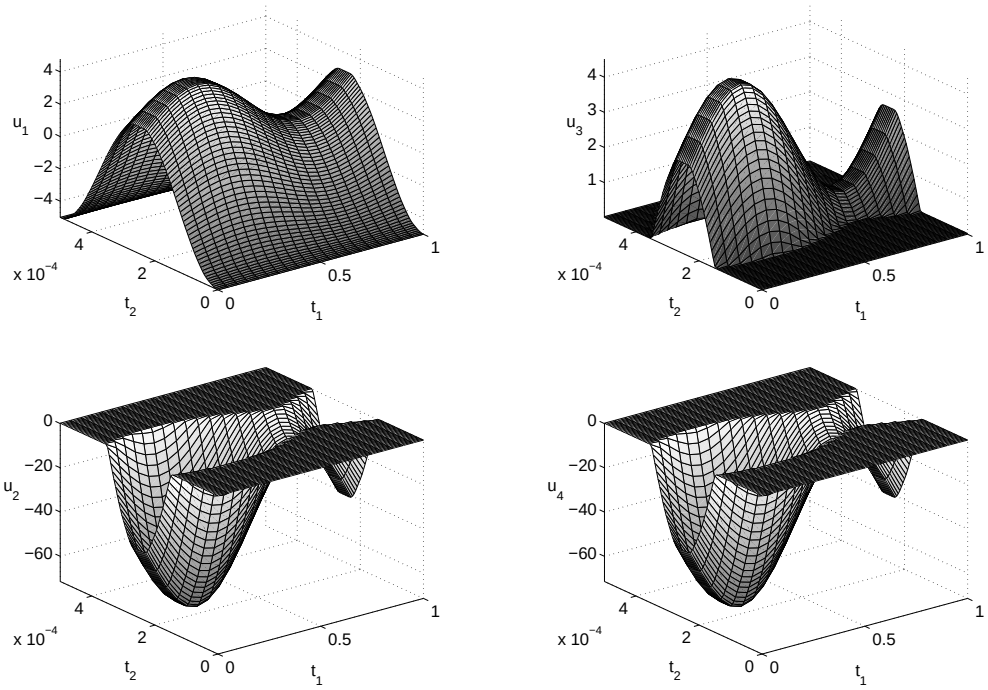

Figure 10: MPDAE solutions of nodes 1 to 4.

Acknowledgements

This work is part of the BMBF programme “Multiskalensysteme in Mikro- und Optoelektronik” within the project “Partielle Differential-Algebraische Multiskalensysteme für die Numerische Simulation von Hochfrequenz-Schaltungen” (No. 03GUNAVN).

References

[1] A. Bartel and S. Knorr, Wavelet-based Adaptive Grids for the Simulation of Multirate Partial Differential-Algebraic Equations, to appear in: PAMM.

[2] H.G. Brachtendorf, G. Welsch, R. Laur and A. Bunse-Gerstner, Numerical steady state analysis of electronic circuits driven by multi-tone signals, Electrical Engineering 79 (1996), 103–112.

[3] A. Cohen, Biorthogonal wavelets, in: Chui, C., (Ed.), Wavelet Analysis and its Applications II: Wavelets - A Tutorial in Theory and Applications, Academic Press, New York (1992), pp. 123–152.

[4] A. Cohen, I. Daubechies and P. Vial, Wavelets on the Interval and Fast Wavelet Transforms, Applied and Computational Harmonic Analysis 1 (1993), 54–81.

[5] M. Günther and U. Feldmann, CAD based electric circuit modeling in industry I: mathematical structure and index of network equations, Surv. Math. Ind. 8 (1999), 97–129.

[6] E. Hairer, S.P. Nørsett and G. Wanner, Solving Ordinary Differential Equations I: Nonstiff Problems, 2nd Ed., Springer, Berlin, 2000.

[7] W. Kampowsky, P. Rentrop and W. Schmitt, Classification and numerical simulation of electric circuits, Surv. Math. Ind. 2 (1992), 23–65.

[8] S. Knorr and U. Feldmann, Simulation of pulsed signals in MPDAE-modelled SC-circuits, in: A. Di Bucchianico, R.M.M. Mattheij and M.A. Peletier, (Eds.), Progress in Industrial Mathematics at ECMI 2004, Mathematics in Industry, Vol. 8, Springer, Berlin, 2006, pp. 159–163.

[9] S. Knorr and M. Günther, Index analysis of multirate partial differential-algebraic systems in RF-circuits, in: A.M. Anile, G. Alì and G. Mascali, (Eds.), Scientific Computing in Electrical Engineering, Mathematics in Industry, Vol. 9, Springer, Berlin, 2006, pp. 93-100.

[10] O. Narayan and J. Roychowdhury, Analyzing oscillators using multitime PDEs, IEEE Trans. CAS I 50/7 (2003), 894–903.

[11] R. Pulch and M. Günther, A method of characteristics for solving multirate partial differential equations in radio frequency application, Appl. Numer. Math. 42 (2002), 397–409.

[12] R. Pulch, Finite difference methods for multi time scale differential algebraic equations, Z. Angew. Math. Mech. 83/9 (2003), 571–583.

[13] R. Pulch, Multi time scale differential equations for simulating frequency modulated signals, Appl. Numer. Math. 53 (2005), 421–436.

[14] J. Roychowdhury, Analysing circuits with widely-separated time scales using numerical PDE methods, IEEE Trans. CAS I 48/5 (2001), 578–594.